Granular Matter 2, 113–121 © Springer-Verlag 2000

A comparison of discrete granular material models with continuous microplane formulations

Ellen Kuhl, Gian Antonio D'Addetta, Hans J. Herrmann, Ekkehard Ramm

Abstract The main objective of this paper is the discussion of two different strategies of simulating the constitutive behavior of granular assemblies. For this, we will focus on discrete particle methods which are widely used in physical science and on continuum–based microplane models which are applied by the engineering community. After deriving the overall constitutive equations based on Voigt's hypothesis, special focus will be dedicated to the comparison of the relations between the microscopic and macroscopic quantities of each model. It will be demonstrated, that the two basically different modelling techniques lead to remarkably similar results for elastic as well as elasto–plastic material behavior.

1 Motivation

The constitutive description of the mechanical behavior of granular systems is of great interest to the fields of geotechnics and various other related applications. By taking into account the discrete nature of the microstructure of a granular assembly, numerous different discrete models have been developed, compare for example Cundall & Strack [1] or Bathurst & Rothenburg [2]. Most of them are based on a finite number of discrete, semi-rigid spherical or polygon-shaped particles interacting by means of contact forces. The specification of an appropriate contact law is probably the most significant part of the discrete model. For example, the contact behavior can be formulated in a linear or nonlinear elastic fashion according to the classical Hertz model or include frictional effects along the line of Coulomb's friction law.

Received: 19 May 1999

E. Kuhl (✉), G. A. D'Addetta, E. Ramm
Institute for Structural Mechanics,
University of Stuttgart,
Pfaffenwaldring 7, 70550 Stuttgart, Germany

H. J. Herrmann
Institute for Computer Applications I,
University of Stuttgart,
Pfaffenwaldring 27, 70550 Stuttgart, Germany

The authors would like to acknowledge the support of the German National Science Foundation DFG through the graduate programme 'Modellierung und Diskretisierungsmethoden für Kontinua & Strömungen' and the DFG research group 'Modellierung kohäsiver Reibungsmaterialien.'

In order to compare the results of the discrete element simulation with macroscopic measurements, different averaging techniques can be applied in order to derive homogenized quantities characterizing the overall behavior of the assembly. Thus, the definition of the macroscopic stress tensor has been studied intensively in the beginning of the 80s and can now be considered as well-established, see Rothenburg & Selvadurai [3] or Christoffersen, Mehrabadi & Nemat-Nasser [4]. During the last decade, various studies have been dedicated to the derivation of explicit expressions for the overall strain tensor, compare Kruyt & Rothenburg [5], and, accordingly, for the macroscopic constitutive moduli Walton [6], Cambou, Dubujet, Emeriault & Sidoroff [7], Emeriault & Cambou [8], Chang [9] and Liao, Chang, Young & Chang [10]. While these homogenization strategies are based on the assumption of an elastic material behavior, dislocation and plastic flow which have been found experimentally by Drescher & de Josselin de Jong [11] are incorporated in more advanced studies, see Chang [12] for example. It should be mentioned, that though the discrete particle models perform excellent for cohesionless granular materials under compressive and shear loading, they have been less applied to tensile failure of cohesive frictional materials like marl, clay or concrete.

While discrete models take into account the individual behavior of each single particle, continuum-based approaches can only describe the material behavior in an average sense. Although, in most cases, the choice of the specific constitutive formulation is motivated by microstructural considerations, the material response is characterized exclusively in terms of stresses or strains and a set of internal variables, which represent microstructural effects in a phenomenological fashion. The microplane plasticity model is a classical representative of this class of continuum–based constitutive models. It is based on the early ideas of Mohr [13], who suggested to characterize the response of a material point by describing its behavior in various representative directions in space. Similar to the particle models, the choice of the constitutive assumption relating the corresponding stress and strain vector of each direction can be considered as the most important feature of the model. The overall response of the material point is obtained by integrating the resulting stress vectors over the entire solid angle. Thus, the microplane concept provides a general framework of reproducing anisotropy in a natural fashion. Its first application to rock–like geomaterials was presented at the end of the 70s by Zienkiewicz

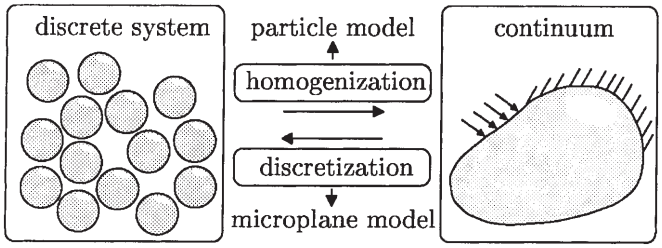

Fig. 1. Relation between discrete and macroscopic model

& Pande [14]. A decade later, a microplane model for cementitious materials was proposed by Bažant & Gambarova [15] and Bažant & Prat [16], which serves as the basis for most existing microplane formulations, compare Carol, Bažant & Prat [17] or Kuhl & Ramm [18].

Figure 1 sketches the relation between the discrete particle model and the continuum–based microplane model. While the particle model is of discrete nature and an overall characterization can only be derived through appropriate homogenization techniques, the microplane model is initially continuous and has to be discretized for computational reasons.

Although derived from two completely different fields, both models show significant similarities from a theoretical point of view. This contribution aims at highlighting the equivalences of the two different material formulations. Therefore, we will start by briefly summarizing the basic ideas of the particle model restricting ourselves to granular assemblies of linear elastic, non–rotating spherical particles. The resulting response of a representative assembly will be derived by means of homogenization techniques based on Voigt's hypothesis. Relations between the macroscopic moduli and the normal and tangential contact stiffness will be pointed out. Secondly, we will recapitulate the constitutive equations of the microplane model. Again, a kinematic constraint according to Voigt's hypothesis is applied in order to determine the relations between the macroscopic and the microplane–based moduli. In chapter 4, both formulations are further enhanced by incorporating elasto–plastic effects. The similarity of the model responses is highlighted by means of the two homogenized tangent operators of similar structure. A comparison and a final discussion of both models will be given in chapter 5.

Note, that the following derivations are based on the assumption of small displacements and small strains, restricting the models to linear kinematics.

2
Discrete model for elastic granular assemblies

2.1
Macroscopic strain tensor – particle displacements

Various techniques of different degree of complexity can be applied in order to determine the homogenized response of a granular assembly. Since the homogenization itself is not the scope of this study, we will restrict ourselves to the application of one of the simplest techniques which is based on Voigt's hypothesis. We will thus assume that the strain $\boldsymbol{\varepsilon}$ is distributed uniformly in the packing. Consequently, every particle within the assembly displaces in accordance with the uniform strain as the mean displacement field. Thus, any vector $\boldsymbol{l}$ connecting two arbitrary points of the assembly is strained by the amount $\Delta\boldsymbol{l}$. This amount of straining can be expressed as the scalar product of the normalized displacement $\boldsymbol{\varepsilon}$, which will be interpreted as the strain tensor in the following, and the vector $\boldsymbol{l}$ itself.

$$\Delta\boldsymbol{l} = \boldsymbol{\varepsilon} \cdot \boldsymbol{l} \tag{1}$$

In particular, this relation holds for the relative displacement $\Delta\boldsymbol{l}^c$ of the contact vector $\boldsymbol{l}^c$ which connects the centers of mass of the two corresponding particles in contact. By expressing the contact vector in terms of its length $||\boldsymbol{l}^c|| = \sqrt{\boldsymbol{l}^c \cdot \boldsymbol{l}^c}$ and the unit normal to the contact plane $\boldsymbol{n}^c = \boldsymbol{l}^c / ||\boldsymbol{l}^c||$, we can rewrite equation (1) in the following form.

$$\Delta\boldsymbol{l}^c(\boldsymbol{n}^c) = ||\boldsymbol{l}^c||\, \boldsymbol{\varepsilon} \cdot \boldsymbol{n}^c \tag{2}$$

Figure 2 indicates that the contact displacement $\Delta\boldsymbol{l}^c$ can be additively decomposed into the displacements normal and tangential to the contact plane.

$$\Delta\boldsymbol{l}^c(\boldsymbol{n}^c) = \Delta l_N^c \boldsymbol{n} + \Delta\boldsymbol{l}_T^c \tag{3}$$

Note, that for this general three dimensional formulation, the direction of tangential displacement is not known in advance. Consequently, tangential displacements are characterized through the vector $\Delta\boldsymbol{l}_T^c$ while the amount of relative displacement in the normal direction is denoted by the scalar–valued quantity Δl_N^c. Both components can be directly related to the overall strain tensor in the following form.

$$\begin{aligned} \Delta l_N^c(\boldsymbol{n}^c) &= ||\boldsymbol{l}^c||\, \boldsymbol{n}^c \cdot \boldsymbol{\varepsilon} \cdot \boldsymbol{n}^c = ||\boldsymbol{l}^c|| \boldsymbol{N}^c : \boldsymbol{\varepsilon} \\ \Delta\boldsymbol{l}_T^c(\boldsymbol{n}^c) &= ||\boldsymbol{l}^c||\, \boldsymbol{\varepsilon} \cdot \boldsymbol{n}^c - \Delta l_N^c \boldsymbol{n}^c = ||\boldsymbol{l}^c|| \boldsymbol{T}^c : \boldsymbol{\varepsilon} \end{aligned} \tag{4}$$

For sake of transparency, we have introduced the second and third order projection tensors $\boldsymbol{N}$ and $\boldsymbol{T}$ as functions of the characteristic direction $\boldsymbol{n}$ and the fourth order unit tensor $\mathscr{I}$ with coefficients $\mathscr{I}_{ijkl} = [\delta_{ik}\delta_{jl} + \delta_{il}\delta_{jk}]/2$.

$$\begin{aligned} \boldsymbol{N}(\boldsymbol{n}) &= \boldsymbol{n} \otimes \boldsymbol{n} \\ \boldsymbol{T}(\boldsymbol{n}) &= \boldsymbol{n} \cdot \mathscr{I} - \boldsymbol{n} \otimes \boldsymbol{n} \otimes \boldsymbol{n} \end{aligned} \tag{5}$$

In order to determine an analytical solution for the stress-strain relationship of a granular assembly, we have to derive integration formulae for the fourth order products of these two tensors. Therefore, we will make use of the following analytical integration formulae of the zeroth, second and fourth order fabric tensors integrated over the

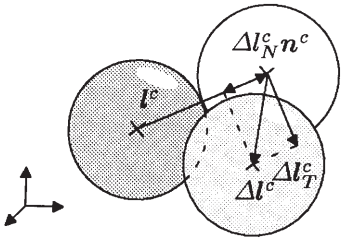

Fig. 2. Normal and tangential displacement of contact vector

solid angle Ω, compare Lubarda & Krajcinovic [19] or Kanatani [20].

$$\begin{aligned} &\tfrac{3}{4\pi}\int_\Omega d\Omega = 3 \\ &\tfrac{3}{4\pi}\int_\Omega \boldsymbol{n}\otimes\boldsymbol{n}\, d\Omega = \mathbf{1} \\ &\tfrac{3}{4\pi}\int_\Omega \boldsymbol{n}\otimes\boldsymbol{n}\otimes\boldsymbol{n}\otimes\boldsymbol{n}\, d\Omega = \tfrac{3}{5}\boldsymbol{\mathcal{I}}^{vol} + \tfrac{2}{5}\boldsymbol{\mathcal{I}} \end{aligned} \tag{6}$$

Herein, $\mathbf{1}$ denotes the second order unit tensor with coefficients $1_{ij} = \delta_{ij}$. Its dyadid product defines the volumetric fourth order unit tensor $\boldsymbol{\mathcal{I}}^{vol} = 1/3\ \mathbf{1}\otimes\mathbf{1}$. Consequently, the fourth order products of the projection tensors $\boldsymbol{N}$ and $\boldsymbol{T}$ show the following properties when integrated analytically over the solid angle Ω,

$$\begin{aligned} &\tfrac{3}{4\pi}\int_\Omega \boldsymbol{N}\otimes\boldsymbol{N}\, d\Omega = \tfrac{3}{5}\boldsymbol{\mathcal{I}}^{vol} + \tfrac{2}{5}\boldsymbol{\mathcal{I}} \\ &\tfrac{3}{4\pi}\int_\Omega \boldsymbol{T}^T\cdot\boldsymbol{T}\, d\Omega = -\tfrac{3}{5}\boldsymbol{\mathcal{I}}^{vol} + \tfrac{3}{5}\boldsymbol{\mathcal{I}} \end{aligned} \tag{7}$$

which we will make use of in the following derivations. Note, that by the transpose of the third order tensor $\boldsymbol{T}$ denoted by $\boldsymbol{T}^T$, we will understand the following expression, $\boldsymbol{T}^T = \boldsymbol{\mathcal{I}}\cdot\boldsymbol{n} - \boldsymbol{n}\otimes\boldsymbol{n}\otimes\boldsymbol{n}$.

2.2 Micromechanical contact law

The normal and the tangential contact forces f_N^c and $\boldsymbol{f}_T^c$ are related to the normal and the tangential contact displacements through the constitutive assumption at the contact. For sake of simplicity, we will assume a linear version of the elastic contact model along the lines of Hertz which takes the following form.

$$\begin{aligned} f_N^c\,(\boldsymbol{n}^c) &= k_N\ \Delta l_N^c \\ \boldsymbol{f}_T^c\,(\boldsymbol{n}^c) &= k_T\ \Delta\boldsymbol{l}_T^c \end{aligned} \tag{8}$$

Herein, k_N and k_T denote the normal and the tangential contact stiffness, respectively. Moreover, we have neglected the rotations of the particles, which is a reasonable assumption for dense packings, compare Bathurst & Rothenburg [2]. As indicated in Figure 3, the normal and the tangential contact force represent the components of the contact force vector $\boldsymbol{f}^c(\boldsymbol{n}^c)$.

$$\boldsymbol{f}^c(\boldsymbol{n}^c) = f_N^c\boldsymbol{n}^c + \boldsymbol{f}_T^c \tag{9}$$

2.3 Contact force – macroscopic stress tensor

The contact forces can be related to the macroscopic stress tensor through the principle of virtual work as demonstrated by Christoffersen, Mehrabadi & Nemat – Nasser [4] and more recently by Chang [9]. The equivalence of the overall macroscopic virtual work and the virtual work of the granular assembly

$$\delta W^{mac} = \delta W^{mic} \tag{10}$$

serves as starting point for the derivation of the macroscopic stress tensor. The macroscopic virtual work δW^{mac} can be expressed as the scalar product of the macroscopic stress tensor $\boldsymbol{\sigma}$ and the virtual strains $\delta\boldsymbol{\varepsilon}$, while the virtual work of the granular assembly is given as the product of all contact forces $\boldsymbol{f}^c$ with the corresponding virtual change of the contact vectors $\delta\Delta\boldsymbol{l}^c$ summed over all contacts c and divided by the volume of the assembly V.

$$\begin{aligned} \delta W^{mac} &= \boldsymbol{\sigma} : \delta\boldsymbol{\varepsilon} \\ \delta W^{mic} &= \frac{1}{V}\sum_{c\in V}\boldsymbol{f}^c\cdot\delta\Delta\boldsymbol{l}^c \end{aligned} \tag{11}$$

Equations (10) and (11) together with the kinematic constraint condition $\delta\Delta\boldsymbol{l}^c = \delta\boldsymbol{\varepsilon}\cdot\boldsymbol{l}^c$ as postulated in (1) yield the following expression for the macroscopic stress tensor.

$$\boldsymbol{\sigma} = \frac{1}{V}\sum_{c\in V}[\boldsymbol{f}^c\otimes\boldsymbol{l}^c]^{sym} \tag{12}$$

Note, that $(\bullet)^{sym} = \left[(\bullet) + (\bullet)^T\right]/2$ extracts only the symmetric part of the corresponding quantity. The stress tensor can thus be understood as the symmetric part of the dyadic product of each contact force $\boldsymbol{f}^c$ with the corresponding contact vector $\boldsymbol{l}^c$ summed over all existing contacts c. It should be noted, that this derivation based on the equivalence of virtual work differs from the derivation presented by Luding, Lätzel & Herrmann [21] which, in general, leads to a non-symmetric stress tensor. However, for the formulation derived herein, the stress tensor is guaranteed to be symmetric by construction. Combining the above definition with the definition of the contact force vector (9), we can rewrite the definition of the stress tensor in the following form.

$$\boldsymbol{\sigma} = \frac{1}{V}\sum_{c\in V}[[f_N^c\boldsymbol{n}^c + \boldsymbol{f}_T^c]\otimes\boldsymbol{l}^c]^{sym} \tag{13}$$

By making use of the following identities $\boldsymbol{l}^c = ||\boldsymbol{l}^c||\ \boldsymbol{n}^c$ and $[\boldsymbol{f}_T^c\otimes\boldsymbol{n}^c]^{sym} = \boldsymbol{T}^{cT}\cdot\boldsymbol{f}_T^c$ we can express the stress tensor in terms of the normal and the tangential contact force, the length of the contact vector and the corresponding projection tensors.

$$\boldsymbol{\sigma} = \frac{1}{V}\sum_{c\in V}||\boldsymbol{l}^c||\left[\boldsymbol{N}^c f_N^c + \boldsymbol{T}^{cT}\cdot\boldsymbol{f}_T^c\right] \tag{14}$$

The combination of the particle contact law (8) and the kinematic constraint (4) with equation (14) yields a formulation in terms of the given contact stiffnesses and the projection tensors and the current strain tensor $\boldsymbol{\varepsilon}$.

$$\boldsymbol{\sigma} = \frac{1}{V}\sum_{c\in V}||\boldsymbol{l}^c||^2\left[k_N\boldsymbol{N}^c\otimes\boldsymbol{N}^c + k_T\boldsymbol{T}^{cT}\cdot\boldsymbol{T}^c\right] : \boldsymbol{\varepsilon} \tag{15}$$

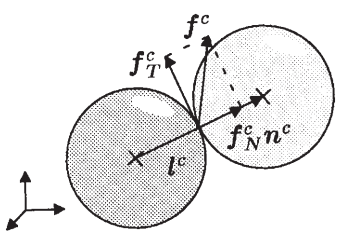

Fig. 3. Normal and tangential components of contact force

2.4 "Discrete" macroscopic constitutive law

The above relation between the overall stress and strain tensor $\boldsymbol{\sigma} = \boldsymbol{\mathscr{C}} : \boldsymbol{\varepsilon}$ leads to the definition of the discrete

fourth order constitutive tensor $\mathscr{C}$ of the granular material.

$$\mathscr{C} = \frac{1}{V} \sum_{c \in V} ||\boldsymbol{l}^c||^2 \left[k_N \boldsymbol{N}^c \otimes \boldsymbol{N}^c + k_T \boldsymbol{T}^{cT} \cdot \boldsymbol{T}^c \right] \tag{16}$$

2.5 Homogenization – continuous constitutive law

In the following, we will demonstrate how an analytical solution for the response of an elastic granular assembly can be derived. We will restrict ourselves to granular materials with an isotropic packing structure, for which the contact points are distributed with uniform probability over all possible directions in space. Moreover, the assembly is assumed to be composed of equally sized particles, for which $\boldsymbol{l}^c = 2r\boldsymbol{n}^c$ with $r = \text{const}$. Consequently, the above definitions for the "discrete" stress tensor and the discrete constitutive moduli can be transformed into an integral form, if a suitably large representative volume with a large number of particles is considered. According to Liao, Chang, Young & Chang [10], the summation of an arbitrary function F over all contacts $c = 1, \ldots, N$ can be expressed through its integral over the solid angle Ω weighted by the number of contacts N divided by 4π.

$$\sum_{c=1}^{N} F(\boldsymbol{n}^c) = \frac{N}{4\pi} \int_{\Omega} F(\boldsymbol{n}) d\Omega \tag{17}$$

Consequently, the continuous form of the stress definition of equation (12) can be expressed as

$$\boldsymbol{\sigma} = \frac{Nr}{2V\pi} \int_{\Omega} [\boldsymbol{f} \otimes \boldsymbol{n}]^{sym} \, d\Omega \tag{18}$$

whereas the continuous counterpart of the tensor of constitutive moduli defined in equation (16) takes the following form.

$$\mathscr{C} = \frac{Nr^2}{V\pi} \int_{\Omega} \left[k_N \boldsymbol{N} \otimes \boldsymbol{N} + k_T \boldsymbol{T}^T \cdot \boldsymbol{T} \right] d\Omega \tag{19}$$

If we postulate a linear elastic contact law which is identical for each contact, the contact stiffnesses k_N and k_T are independent of the direction $\boldsymbol{n}$ and can therefore be written in front of the integral.

$$\mathscr{C} = k_N \frac{Nr^2}{V\pi} \int_{\Omega} \boldsymbol{N} \otimes \boldsymbol{N} d\Omega + k_T \frac{Nr^2}{V\pi} \int_{\Omega} \boldsymbol{T}^T \cdot \boldsymbol{T} \, d\Omega \tag{20}$$

It remains to apply the integration formulae of the fourth order products of the projection tensors we had summarized in equation (7). By comparing the result of the integration with the generalized form of Hooke's law for a linear elastic material,

$$\begin{aligned} \mathscr{C} &= \frac{4Nr^2}{5V} [k_N - k_T] \mathscr{I}^{vol} + \frac{4Nr^2}{15V} [2k_N + 3k_T] \mathscr{I} \\ \mathscr{C} &= 3\lambda \mathscr{I}^{vol} + 2\mu \mathscr{I} \end{aligned} \tag{21}$$

we can easily express the Lamé constants λ and μ in terms of the contact stiffnesses k_N and k_T,

$$\lambda = \frac{4Nr^2}{15V} [k_N - k_T] \quad \text{and} \quad \mu = \frac{4Nr^2}{15V} \left[k_N + \frac{3}{2} k_T \right] \tag{22}$$

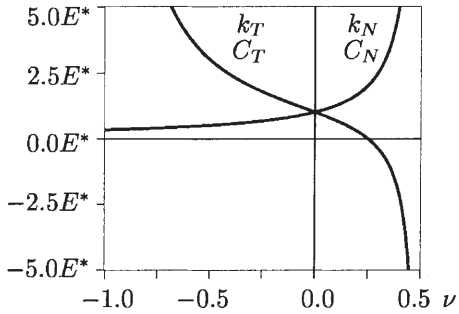

Fig. 4. Contact stiffnesses as a function of Poisson's ratio

or, equivalently, formulate Young's modulus and Poisson's ratio as functions of the contact stiffnesses.

$$E = \frac{4Nr^2}{3V} \frac{k_N [2k_N + 3k_T]}{4k_N + k_T} \quad \text{and} \quad \nu = \frac{k_N - k_T}{4k_N + k_T} \tag{23}$$

From a physical point of view, the value of Poisson's ratio can lie within the range of $-1 \leq \nu \leq 1/2$. However, the constitutive equations derived above are restricted to a material with Poisson's ratio of $-1 \leq \nu \leq 1/4$, as can be concluded from equation (23). A larger value for Poisson's ratio can only be obtained, if the tangential stiffness becomes negative, which is a non-reasonable assumption from a physical point of view. Figure 4 illustrates this drawback of the model. It shows the normal and tangential contact stiffnesses for different Poisson ratios. Their values are scaled by the modified Young's modulus $E^* = [3V/4Nr^2] E$. If the macroscopic moduli measured in an experiment are found to lie within this limited range, the corresponding contact stiffnesses can be expressed in the following form.

$$k_N = \frac{3V}{4Nr^2} [2\mu + 3\lambda] \quad \text{and} \quad k_T = \frac{3V}{4Nr^2} [2\mu - 2\lambda] \tag{24}$$

$$k_N = \frac{3V}{4Nr^2} \frac{E}{1 - 2\nu} \quad \text{and} \quad k_T = \frac{3V}{4Nr^2} \frac{E}{1 + \nu} \frac{1 - 4\nu}{1 - 2\nu} \tag{25}$$

3 Continuum-based elastic microplane model

3.1 Macroscopic strain tensor – microplane strains

Continuum models are based on the assumption that the displacement field is continuous throughout the whole domain of consideration. With a given displacement field $\boldsymbol{u}$, the corresponding strain field $\boldsymbol{\varepsilon}$ can be determined as the symmetric part of the displacement gradient

$$\boldsymbol{\varepsilon} = \nabla^{sym} \boldsymbol{u} \tag{26}$$

if we restrict ourselves to the small displacement and small strain case. In analogy to the discrete model described in the previous section, we will apply a kinematic constraint, assuming that the strains are distributed equally in space. Consequently, the strain vector $\boldsymbol{t}_\varepsilon$ associated with the direction characterized through the normal $\boldsymbol{n}$ is given in the following form.

$$\boldsymbol{t}_\varepsilon(\boldsymbol{n}) = \boldsymbol{\varepsilon} \cdot \boldsymbol{n} \tag{27}$$

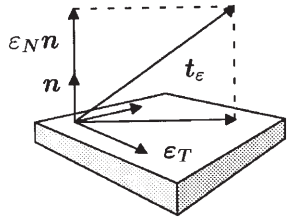

Fig. 5. Normal and tangential strains on microplane

This strain vector can be additively decomposed into a normal and a tangential contribution ε_N and $\boldsymbol{\varepsilon}_T$ as illustrated in Figure 5,

$$\boldsymbol{t}_\varepsilon(\boldsymbol{n}) = \varepsilon_N \boldsymbol{n} + \boldsymbol{\varepsilon}_T \tag{28}$$

whereby the normal strain component and the tangential strain vector are given as follows.

$$\begin{aligned} \varepsilon_N(\boldsymbol{n}) &= \boldsymbol{n} \cdot \boldsymbol{\varepsilon} \cdot \boldsymbol{n} = \boldsymbol{N} : \boldsymbol{\varepsilon} \\ \boldsymbol{\varepsilon}_T(\boldsymbol{n}) &= \boldsymbol{\varepsilon} \cdot \boldsymbol{n} - \varepsilon_N \boldsymbol{n} = \boldsymbol{T} : \boldsymbol{\varepsilon} \end{aligned} \tag{29}$$

3.2 Microplane constitutive law

Again, for sake of transparency, we will first assume a linear elastic material behavior. Consequently, the microplane stresses σ_N and $\boldsymbol{\sigma}_T$ can be expressed exclusively in terms of the normal strain ε_N, the tangential strain vector $\boldsymbol{\varepsilon}_T$ and the normal and tangential elasticity modulus of the corresponding plane C_N and C_T.

$$\begin{aligned} \sigma_N(\boldsymbol{n}) &= C_N \, \varepsilon_N \\ \boldsymbol{\sigma}_T(\boldsymbol{n}) &= C_T \, \boldsymbol{\varepsilon}_T \end{aligned} \tag{30}$$

Note, that we have applied the additional assumption of microplane isotropy by introducing only a scalar-valued tangential elasticity modulus. As a natural consequence, the tangential stress vector will always remain parallel to the tangential strain vector, $\boldsymbol{\sigma}_T \,||\, \boldsymbol{\varepsilon}_T$. The resulting traction vector $\boldsymbol{t}_\sigma$ of the plane can thus be expressed in terms of its normal and tangential components as indicated in Figure 6.

$$\boldsymbol{t}_\sigma(\boldsymbol{n}) = \sigma_N \boldsymbol{n} + \boldsymbol{\sigma}_T \tag{31}$$

3.3 Microplane stresses – macroscopic stress tensor

Again, we will make use of the equivalence of the macroscopic and the microplane–based virtual work

$$\delta W^{mac} = \delta W^{mic} \tag{32}$$

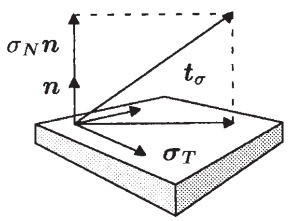

Fig. 6. Normal and tangential stresses on microplane

in order to determine the overall stress tensor. According to equation (11), the macroscopic virtual work is given as the scalar product of the macroscopic stresses $\boldsymbol{\sigma}$ and the virtual strain tensor $\delta\boldsymbol{\varepsilon}$, whereas the microplane–based virtual work can be expressed as the product of the traction vector $\boldsymbol{t}_\sigma$ and the virtual strain vector $\delta\boldsymbol{t}_\varepsilon$ integrated over the solid angle Ω, compare (6).

$$\begin{aligned} \delta W^{mac} &= \boldsymbol{\sigma} : \delta\boldsymbol{\varepsilon} \\ \delta W^{mic} &= \frac{3}{4\pi} \int_\Omega \boldsymbol{t}_\sigma \cdot \delta\boldsymbol{t}_\varepsilon \, d\Omega \end{aligned} \tag{33}$$

Together with the kinematic constraint condition of equation (29), such that $\delta\boldsymbol{t}_\varepsilon = \delta\boldsymbol{\varepsilon} \cdot \boldsymbol{n}$, equations (32) and (33) yield the definition of the macroscopic stress tensor as a function of the stress vector and the plane's normal.

$$\boldsymbol{\sigma} = \frac{3}{4\pi} \int_\Omega [\boldsymbol{t}_\sigma \otimes \boldsymbol{n}]^{sym} \, d\Omega \tag{34}$$

Making use of the definition of the stress vector (31)

$$\boldsymbol{\sigma} = \frac{3}{4\pi} \int_\Omega [[\sigma_N \boldsymbol{n} + \boldsymbol{\sigma}_T] \otimes \boldsymbol{n}]^{sym} \, d\Omega \tag{35}$$

and the algebraic equivalence of $[\boldsymbol{\sigma}_T \otimes \boldsymbol{n}]^{sym} = \boldsymbol{T}^T \cdot \boldsymbol{\sigma}_T$, we obtain the definition of the macroscopic stress tensor in terms of the microscopic stress components and the projection tensors.

$$\boldsymbol{\sigma} = \frac{3}{4\pi} \int_\Omega \big[\boldsymbol{N}\sigma_N + \boldsymbol{T}^T \cdot \boldsymbol{\sigma}_T\big] d\Omega \tag{36}$$

The overall macroscopic constitutive relation can be derived by inserting the definition of the microplane stresses (30) into (36) yielding the following relation.

$$\boldsymbol{\sigma} = \frac{3}{4\pi} \int_\Omega \big[C_N \boldsymbol{N} \otimes \boldsymbol{N} + C_T \boldsymbol{T}^T \cdot \boldsymbol{T}\big] d\Omega : \boldsymbol{\varepsilon} \tag{37}$$

3.4 Continuous macroscopic constitutive law

The continuous fourth order tensor of constitutive moduli relating the macroscopic stresses and strains as $\boldsymbol{\sigma} = \boldsymbol{\mathscr{C}} : \boldsymbol{\varepsilon}$ can easily be extracted from the above relation.

$$\boldsymbol{\mathscr{C}} = \frac{3}{4\pi} \int_\Omega \big[C_N \boldsymbol{N} \otimes \boldsymbol{N} + C_T \boldsymbol{T}^T \cdot \boldsymbol{T}\big] d\Omega \tag{38}$$

If we assume an isotropic material behavior, the elastic moduli of the microplane are independent of the orientation and can thus be written in front of the integrals.

$$\boldsymbol{\mathscr{C}} = C_N \frac{3}{4\pi} \int_\Omega \boldsymbol{N} \otimes \boldsymbol{N} \, d\Omega + C_T \frac{3}{4\pi} \int_\Omega \boldsymbol{T}^T \cdot \boldsymbol{T} \, d\Omega \tag{39}$$

Again, by applying the integration formulae (7) to calculate the integrals over the solid angle as depicted in Figure 7, we can compare the result of the analytical integration with the generalized form of HOOKE's law,

$$\begin{aligned} \boldsymbol{\mathscr{C}} &= \left[\frac{3}{5}C_N - \frac{3}{5}C_T\right] \boldsymbol{\mathscr{I}}^{vol} + \left[\frac{2}{5}C_N + \frac{3}{5}C_T\right] \boldsymbol{\mathscr{I}} \\ \boldsymbol{\mathscr{C}} &= 3\lambda \boldsymbol{\mathscr{I}}^{vol} + 2\mu \boldsymbol{\mathscr{I}} \end{aligned} \tag{40}$$

yielding the following relation for the Lamé constants

$$\lambda = \frac{1}{5}\left[C_N - C_T\right] \quad \text{and} \quad \mu = \frac{1}{5}\left[C_N + \frac{3}{2}C_T\right] \tag{41}$$

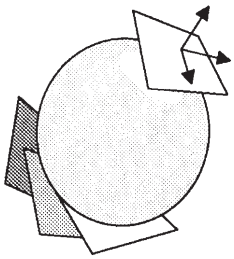

Fig. 7. Continuous model – surface of a unitsphere

as well as the engineering constants of YOUNG's modulus and POISSON's ratio in terms of the elastic microplane moduli C_N and C_T.

$$E = \frac{C_N\,[2C_N + 3C_T]}{4C_N + C_T} \quad \text{and} \quad \nu = \frac{C_N - C_T}{4C_N + C_T} \tag{42}$$

Note, that again, the model is restricted to values of POISSON's ratio lying in the range of $-1 \leq \nu \leq 1/4$. In order to cover the whole range of POISSON's ratio, an additional split of the normal microplane component into normal volumetric and normal deviatoric contributions can be performed as proposed by BAŽANT & GAMBAROVA [15]. If the macroscopic moduli are known from an experiment, the microplane moduli can be determined with the help of the following formulae.

$$C_N = 2\mu + 3\lambda \quad \text{and} \quad C_T = 2\mu - 2\lambda \tag{43}$$

$$C_N = \frac{E}{1-2\nu} \quad \text{and} \quad C_T = \frac{E}{1+\nu}\frac{1-4\nu}{1-2\nu}\ . \tag{44}$$

The values of the elastic microplane moduli for varying POISSON's ratios are depicted in Figure 4, whereby the vertical axis is scaled by YOUNG's modulus $E^* = E$.

3.5
Discretization – microplane–based constitutive law

For the linear elastic isotropic material model derived in the previous section, the integration over the solid angle can be carried out analytically. For an inelastic material behavior, however, this analytical integration becomes nearly impossible. Consequently, the integral expression is commonly evaluated numerically by replacing the integral by a discrete sum evaluated at a certain number of integration points, $c = 1, \ldots, n_{mp}$, and weighted by the weighting coefficients w^c.

$$\int_\Omega F(\boldsymbol{n})d\Omega \approx \sum_{c=1}^{n_{mp}} F(\boldsymbol{n}^c)w^c \tag{45}$$

Consequently, the definition of the macroscopic stress tensor of equation (34) can be approximated by the following sum,

$$\boldsymbol{\sigma} \approx \sum_{c=1}^{n_{mp}} \left[\boldsymbol{t}_\sigma^c \otimes \boldsymbol{n}^c\right]^{sym} w^c \tag{46}$$

whereas the fourth order constitutive tensor defined in equation (38) can be approximated as follows.

$$\mathscr{C} \approx \sum_{c=1}^{n_{mp}} \left[C_N^c \boldsymbol{N}^c \otimes \boldsymbol{N}^c + C_T^c \boldsymbol{T}^{cT} \cdot \boldsymbol{T}^c\right] w^c \tag{47}$$

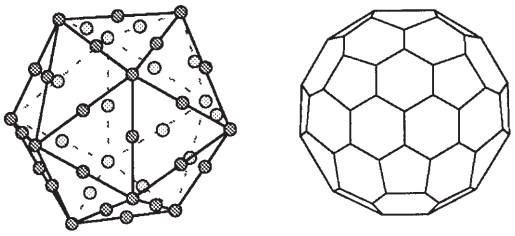

Fig. 8. Discrete model – polyhedron with 42 microplanes

Obviously, the number of integration points determines the order of accuracy of the approximation. By comparing some of the various different integration formulae for the integration over a solid angle, BAŽANT & OH [22] have found, that the integration with 42 integration points as depicted in Figure 8 yields a sufficiently accurate approximation at an acceptable level of effort.

4
Extension to elasto–plasticity

While the derivations in chapters 2 and 3 were based on an elastic material behavior, this chapter aims at formulating elasto–plastic constitutive equations for both types of models. First, the homogenized response of frictional assemblies is derived. It is based on irreversible contact displacements which were verified experimentally by investigations of DRESCHER & DE JOSSELIN DE JONG [11]. In the second part of this chapter, the derivation of an elasto-plastic version of the microplane model is presented.

4.1
Granular assembly with frictional contacts

Frictional contact laws for granular assemblies are based on the idea that the normal and tangential components of the contact displacement can be additively decomposed into reversible elastic parts denoted by Δl_N^{el} and $\Delta \boldsymbol{l}_T^{el}$ and irreversible plastic contributions Δl_N^{pl} and $\Delta \boldsymbol{l}_T^{pl}$.

$$\begin{aligned} \Delta l_N(\boldsymbol{n}) &= \Delta l_N^{el} + \Delta l_N^{pl} \\ \Delta \boldsymbol{l}_T(\boldsymbol{n}) &= \Delta \boldsymbol{l}_T^{el} + \Delta \boldsymbol{l}_T^{pl} \end{aligned} \tag{48}$$

The normal and tangential components of the contact force can be expressed exclusively in terms of the elastic contact displacements.

$$\begin{aligned} f_N(\boldsymbol{n}) &= k_N \Delta l_N^{el} = k_N \Delta l_N - f_N^{pl} \quad f_N^{pl} := k_N \Delta l_N^{pl} \\ \boldsymbol{f}_T(\boldsymbol{n}) &= k_T \Delta \boldsymbol{l}_T^{el} = k_T \Delta \boldsymbol{l}_T - \boldsymbol{f}_T^{pl} \quad \boldsymbol{f}_T^{pl} := k_T \Delta \boldsymbol{l}_T^{pl} \end{aligned} \tag{49}$$

The cohesionless frictional sliding of the particles is characterized through COULOMB's friction law, which motivates the introduction of a yield function Φ of the following form.

$$\Phi(\boldsymbol{n}) = ||\,\boldsymbol{f}_T\,|| - \tan\varphi\, f_N \leq 0 \tag{50}$$

Note, that a coupling of the normal and the tangential components of the contact force is introduced through the friction angle φ. The normals to the yield function can thus be expressed as follows.

$$\begin{aligned} \nu_N(\boldsymbol{n}) &:= \partial\Phi/\partial f_N \\ \boldsymbol{\nu}_T(\boldsymbol{n}) &:= \partial\Phi/\partial \boldsymbol{f}_T \end{aligned} \tag{51}$$

The evolution of the plastic contact displacements can be expressed in terms of the plastic multiplier γ and the directions of plastic displacement μ_N and $\boldsymbol{\mu}_T$.

$$\begin{aligned} \Delta\dot{l}_N^{pl}(\boldsymbol{n}) &= \dot{\gamma}\ \mu_N \\ \Delta\dot{\boldsymbol{l}}_T^{pl}(\boldsymbol{n}) &= \dot{\gamma}\ \boldsymbol{\mu}_T \end{aligned} \tag{52}$$

Only in case of an associated friction model, these directions correspond to the normals to the yield function such that $\mu_N = \nu_N$ and $\boldsymbol{\mu}_T = \boldsymbol{\nu}_T$. In general, however, the directions of plastic displacement can be chosen independently yielding a non-associated friction law. In most existing formulations in the literature, the following choice is applied, $\mu_N = 0$ and $\boldsymbol{\mu}_T = \boldsymbol{\nu}_T$, while the normals to the yield surface ν_N and $\boldsymbol{\nu}_T$ remain as defined in equation (51). The sliding process is further characterized through KUHN-TUCKER conditions and the consistency condition.

$$\Phi \leq 0 \quad \dot{\gamma} \geq 0 \quad \Phi\,\dot{\gamma} = 0 \quad \dot{\Phi}\,\dot{\gamma} = 0 \tag{53}$$

The evaluation of the consistency condition (53.4), yields the evolution equation for the plastic multiplier γ

$$\dot{\gamma}(\boldsymbol{n}) = \frac{||\,\boldsymbol{l}\,||}{h}\,[\nu_N k_N \boldsymbol{N} + \boldsymbol{\nu}_T \cdot k_T \boldsymbol{T}] : \dot{\boldsymbol{\varepsilon}} \tag{54}$$

with

$$h(\boldsymbol{n}) := \nu_N k_N \mu_N + \boldsymbol{\nu}_T \cdot k_T \boldsymbol{\mu}_T \ . \tag{55}$$

Consequently, for the case of frictional sliding with the flow directions $\mu_N = 0$ and $\boldsymbol{\mu}_T = \boldsymbol{\nu}_T$ the rate of the normal and tangential plastic contact forces of equation (49) take the following form.

$$\begin{aligned} \dot{f}_N^{pl}(\boldsymbol{n}) &= 0 \\ \dot{\boldsymbol{f}}_T^{pl}(\boldsymbol{n}) &= \left[||\,\dot{\boldsymbol{f}}_T\,|| - \tan\varphi \dot{f}_N\right] \boldsymbol{\mu}_T \end{aligned} \tag{56}$$

Although derived in a different way, these evolution equations correspond to the ones given in the literature, compare for example CHANG [12]. Finally, we can specify the macroscopic stress tensor, which can again be derived by applying the principle of virtual work. It can be expressed in accordance with equation (12),

$$\boldsymbol{\sigma} = \frac{1}{V} \sum_{c \in V} ||\boldsymbol{l}^c||\,[\boldsymbol{f}^c \otimes \boldsymbol{n}^c]^{sym} \tag{57}$$

whereby $\boldsymbol{f}^c = f_N^c \boldsymbol{n} + \boldsymbol{f}_T^c$ denotes the contact vector whose components are specified in equation (49). Moreover, we obtain the definition of the overall tangent operator $\mathscr{C}_{tan}^{ep}$ which relates the resulting macroscopic stress rates to the macroscopic strain rates, $\dot{\boldsymbol{\sigma}} = \mathscr{C}_{tan}^{ep} : \dot{\boldsymbol{\varepsilon}}$. For a discrete granular assembly, the tangent operator can be expressed as follows,

$$\begin{aligned} \mathscr{C}_{tan}^{ep} \ = \mathscr{C}^{el} - \frac{1}{V} \sum_{c \in V} \frac{||\boldsymbol{l}^c||^2}{h}\ [\ \boldsymbol{N}^c k_N \nu_N^c + \boldsymbol{T}^{cT} \cdot k_T \boldsymbol{\nu}_T^c\ ] \\ \otimes [\ \mu_N^c k_N \boldsymbol{N}^c + \boldsymbol{\mu}_T^c \cdot k_T \boldsymbol{T}^c\ ] \end{aligned} \tag{58}$$

with $\mathscr{C}^{el}$ denoting the elasticity tensor of the granular assembly which was derived in equation (16).

4.2
Microplane model for elasto-plastic materials

Similar to the frictional contact laws of granular assemblies, the microplane–based plasticity model is based on the additive decomposition of the microplane strains into elastic and plastic parts.

$$\begin{aligned} \varepsilon_N(\boldsymbol{n}) &= \varepsilon_N^{el} + \varepsilon_N^{pl} \\ \boldsymbol{\varepsilon}_T(\boldsymbol{n}) &= \boldsymbol{\varepsilon}_T^{el} + \boldsymbol{\varepsilon}_T^{pl} \end{aligned} \tag{59}$$

Again, the microplane stresses are assumed to depend only on the elastic parts of the strain components.

$$\begin{aligned} \sigma_N(\boldsymbol{n}) &= C_N \varepsilon_N^{el} \\ \boldsymbol{\sigma}_T(\boldsymbol{n}) &= C_T\ \boldsymbol{\varepsilon}_T^{el} \end{aligned} \tag{60}$$

Moreover, a yield function Φ of DRUCKER–PRAGER type is introduced. It can be expressed as the difference of an equivalent stress $||\,\boldsymbol{\sigma}_T\,|| - \tan\varphi\sigma_N$ and the yield stress Y, which is assumed to be constant in case of ideal plasticity.

$$\Phi(\boldsymbol{n}) = ||\,\boldsymbol{\sigma}_T\,|| - \tan\varphi\,\sigma_N - Y \leq 0 \tag{61}$$

Herein, φ denotes the angle of internal friction whereas the normals to the yield function will be denoted by ν_N and $\boldsymbol{\nu}_T$.

$$\begin{aligned} \nu_N\ (\boldsymbol{n}) &:= \partial\Phi/\partial\sigma_N \\ \boldsymbol{\nu}_T\ (\boldsymbol{n}) &:= \partial\Phi/\partial\boldsymbol{\sigma}_T \end{aligned} \tag{62}$$

The evolution of the plastic strains is determined by the plastic multiplier γ and the normal and tangential flow directions characterized through μ_N and $\boldsymbol{\mu}_T$, respectively.

$$\begin{aligned} \dot{\varepsilon}_N^{pl}(\boldsymbol{n}) &= \dot{\gamma}\ \mu_N \\ \dot{\boldsymbol{\varepsilon}}_T^{pl}(\boldsymbol{n}) &= \dot{\gamma}\ \boldsymbol{\mu}_T \end{aligned} \tag{63}$$

For an associated plasticity model, these flow directions are identical to the corresponding normals to the yield surface, such that $\mu_N = \nu_N$ and $\boldsymbol{\mu}_T = \boldsymbol{\nu}_T$. The loading–unloading process is governed by the KUHN–TUCKER conditions and the consistency condition.

$$\Phi \leq 0 \quad \dot{\gamma} \geq 0 \quad \Phi\,\dot{\gamma} = 0 \quad \dot{\Phi}\,\dot{\gamma} = 0 \tag{64}$$

The evolution of the plastic multiplier can be directly determined from the evaluation of the consistency condition (64.4) such that

$$\dot{\gamma}(\boldsymbol{n}) = \frac{1}{h}\,[\nu_N C_N \boldsymbol{N} + \boldsymbol{\nu}_T \cdot C_T \boldsymbol{T}] : \dot{\boldsymbol{\varepsilon}} \tag{65}$$

with

$$h(\boldsymbol{n}) := \nu_N C_N \mu_N + \boldsymbol{\nu}_T \cdot C_T \boldsymbol{\mu}_T. \tag{66}$$

Consequently, the macroscopic stress tensor is given as the symmetric part of the dyadic product of the traction vector with the corresponding normal,

$$\boldsymbol{\sigma} = \frac{3}{4\pi} \int_\Omega [\boldsymbol{t}_\sigma \otimes \boldsymbol{n}]^{sym}\, d\Omega \tag{67}$$

whereby the components of the traction vector $\boldsymbol{t}_\sigma = \sigma_N \boldsymbol{n} + \boldsymbol{\sigma}_T$ are defined in equations (60). Moreover, the continuous elasto–plastic tangent operator $\mathscr{C}_{tan}^{ep}$ relating the macroscopic stress and strain rates according to $\dot{\boldsymbol{\sigma}} = \mathscr{C}_{tan}^{ep} : \dot{\boldsymbol{\varepsilon}}$ can be expressed in the following form

$$\begin{aligned} \mathscr{C}_{tan}^{ep} = \mathscr{C}^{el} - \frac{3}{4\pi} \int_\Omega \frac{1}{h}\ [\ \boldsymbol{N} C_N \nu_N + \boldsymbol{T}^T \cdot C_T \boldsymbol{\nu}_T\ ] \\ \otimes [\ \mu_N C_N \boldsymbol{N} + \boldsymbol{\mu}_T \cdot C_T \boldsymbol{T}\ ] d\Omega \end{aligned} \tag{68}$$

whereby $\mathscr{C}^{el}$ denotes the elastic constitutive tensor of (38).

4.3 Example

The features of the elasto–plastic material model will be demonstrated by means of a microplane simulation of the two classical model problems of uniaxial compression (Figure 9, right) and simple shear (Figure 9, left). A plane strain situation is assumed. In accordance with most existing particle models from the literature, the yield stress has been set to zero $Y = 0$ N/mm^2, the friction angle has been chosen to $\varphi = 30°$ and a non-associated flow rule with $\mu_N = 0$ and $\boldsymbol{\mu}_T = \boldsymbol{\nu}_T$ has been assumed. Consequently, the model response will correspond to the one of COULOMB type particle models of equally-sized spheres with a uniform contact distribution. Figures 10 and 11 depict the distribution of the plastic multiplier γ characterizing the amount of plastic sliding associated with the normal of the corresponding plane. For each problem, three different ratios of the normal and the tangential elastic contact stiffness have been studied, manifesting themselves in three different values of the macroscopic POISSON's ratio with YOUNG's modulus constant at $E = 30000$ N/mm^2. As expected, for the case of uniaxial compression depicted in Figure 10, maximum sliding takes place normal to the loading direction. Obviously, the amount of sliding increases with increasing POISSON ratios. The response under simple shear is characterized by the REYNOLD's effect introduced through the lateral confinement due to the boundary conditions. Consequently, plastic sliding tends to concentrate under an angle of 45° towards the loading axis, compare Figure 11. Again, the amount of sliding increases with increasing POISSON ratios. This example provides inside into the anisotropic nature of plastic slip in granular media. However, it can only be considered a first step since it is restricted to equally-sized particles with an isotropic contact distribution.

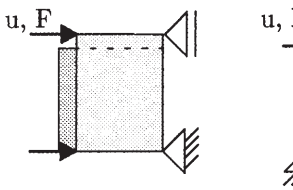

Fig. 9. Geometry of model problems

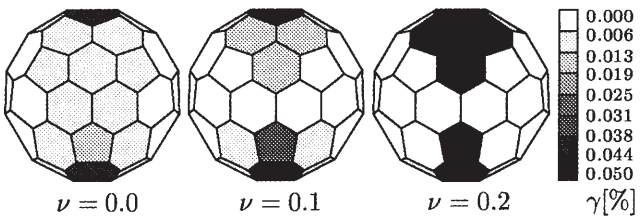

Fig. 10. Uniax. compression – distribution of plastic multiplier

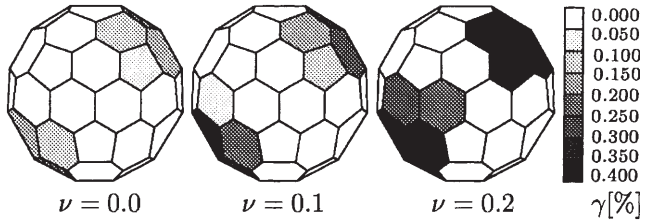

Fig. 11. Simple shear – distribution of plastic multiplier

5 Comparison

Although derived from two completely different fields, the constitutive equations of the discrete particle model and the continuum–based microplane model show various similarities. In both cases, the kinematic relation between the microscopic and the macroscopic quantities was assumed in accordance with VOIGT's hypothesis. While the particle model is formulated in terms of relative displacements and contact forces, the microplane model is based on strain and stress vectors. Consequently, the material parameters of the particle model can be interpreted as normal and tangential contact stiffnesses, whereas the related microplane parameters can be understood as normal and tangential elastic moduli. In both cases, the macroscopic stress tensor is derived through the principle of virtual work. A comparison of the most important equations of both models is summarized in Table 1.

Even for frictional materials, both models show a similar behavior. The particle model is usually associated with COULOMB's friction law for cohesionless materials, whereas the yield function of the microplane model can be introduced in a more general DRUCKER–PRAGER based fashion. It includes not only the difference of the norm of the tangential stress and the normal stress weighted by the friction angle but also a yield stress, which does usually not exist for the particle model. If both material models are written in a similar notation, the existing particle models for frictional sliding can be interpreted as a special case of a non–associated plasticity formulation. Based on the introduction of plastic multipliers, a homogenized tangent operator for the particle model can be derived in the same fashion as for the microplane plasticity model. The remarkable similarity of both formulations is documented in Table 2.

Finally, it should be mentioned, that although there are numerous similarities between both formulations,

Table 1. Comparison of linear elastic models

Granular assembly	Microplane model
$\Delta \boldsymbol{l}^c = \Delta l_N^c \boldsymbol{n} + \Delta \boldsymbol{l}_T^c$	$\boldsymbol{t}_\varepsilon = \varepsilon_N \boldsymbol{n} + \boldsymbol{\varepsilon}_T$
$\Delta l_N^c = \|\|\boldsymbol{l}^c\|\| \boldsymbol{N} : \boldsymbol{\varepsilon}$	$\varepsilon_N = \boldsymbol{N} : \boldsymbol{\varepsilon}$
$\Delta \boldsymbol{l}_T^c = \|\|\boldsymbol{l}^c\|\| \boldsymbol{T} : \boldsymbol{\varepsilon}$	$\boldsymbol{\varepsilon}_T = \boldsymbol{T} : \boldsymbol{\varepsilon}$
$\boldsymbol{f}^c = f_N^c \boldsymbol{n} + \boldsymbol{f}_T^c$	$\boldsymbol{t}_\sigma = \sigma_N \boldsymbol{n} + \boldsymbol{\sigma}_T$
$f_N^c = k_N \Delta l_N^c$	$\sigma_N = C_N \varepsilon_N$
$\boldsymbol{f}_T^c = k_T \Delta \boldsymbol{l}_T^c$	$\boldsymbol{\sigma}_T = C_T \boldsymbol{\varepsilon}_T$
$\boldsymbol{\sigma} = \frac{Nr}{2V\pi} \int [\boldsymbol{f}^c \otimes \boldsymbol{n}]^{sym} \, d\Omega$	$\boldsymbol{\sigma} = \frac{3}{4\pi} \int [\boldsymbol{t}_\sigma \otimes \boldsymbol{n}]^{sym} \, d\Omega$
$k_N = \frac{3V}{4Nr^2} [2\mu + 3\lambda]$	$C_N = 2\mu + 3\lambda$
$k_T = \frac{3V}{4Nr^2} [2\mu - 2\lambda]$	$C_T = 2\mu - 2\lambda$
$\mathscr{C} = \frac{Nr^2}{V\pi} \int [k_N \boldsymbol{N} \otimes \boldsymbol{N} + k_T \boldsymbol{T}^T \cdot \boldsymbol{T}] \, d\Omega$	$\mathscr{C} = \frac{3}{4\pi} \int [C_N \boldsymbol{N} \otimes \boldsymbol{N} + C_T \boldsymbol{T}^T \cdot \boldsymbol{T}] \, d\Omega$

Table 2. Comparison of elasto-plastic models

Granular assembly	Microplane model
$\Delta \boldsymbol{l} = \Delta l_N \boldsymbol{n} + \Delta \boldsymbol{l}_T$	$\boldsymbol{t}_\varepsilon = \varepsilon_N \boldsymbol{n} + \boldsymbol{\varepsilon}_T$
$\Delta l_N = \Delta l_N^{el} + \Delta l_N^{pl}$	$\varepsilon_N = \varepsilon_N^{el} + \varepsilon_N^{pl}$
$\Delta \boldsymbol{l}_T = \Delta \boldsymbol{l}_T^{el} + \Delta \boldsymbol{l}_T^{pl}$	$\boldsymbol{\varepsilon}_T = \boldsymbol{\varepsilon}_T^{el} + \boldsymbol{\varepsilon}_T^{pl}$
$\boldsymbol{f} = f_N \boldsymbol{n} + \boldsymbol{f}_T$	$\boldsymbol{t}_\sigma = \sigma_N \boldsymbol{n} + \boldsymbol{\sigma}_T$
$f_N = k_N \Delta l_N^{el}$	$\sigma_N = C_N \varepsilon_N^{el}$
$\boldsymbol{f}_T = k_T \Delta \boldsymbol{l}_T^{el}$	$\boldsymbol{\sigma}_T = C_T \boldsymbol{\varepsilon}_T^{el}$
$\boldsymbol{\sigma} = \frac{Nr}{2V\pi} \int [\boldsymbol{f} \otimes \boldsymbol{n}]^{sym} \, d\Omega$	$\boldsymbol{\sigma} = \frac{3}{4\pi} \int [\boldsymbol{t}_\sigma \otimes \boldsymbol{n}]^{sym} \, d\Omega$
$\Phi = f^{eq} \leq 0$	$\Phi = \sigma^{eq} - Y \leq 0$
$f^{eq} = \|\|\boldsymbol{f}_T\|\| - \tan\varphi f_N$	$\sigma^{eq} = \|\|\boldsymbol{\sigma}_T\|\| - \tan\varphi \sigma_N$
$\Delta \dot{l}_N^{pl} = \dot{\gamma} \, \mu_N$	$\dot{\varepsilon}_N^{pl} = \dot{\gamma} \, \mu_N$
$\Delta \dot{\boldsymbol{l}}_T^{pl} = \dot{\gamma} \, \boldsymbol{\mu}_T$	$\dot{\boldsymbol{\varepsilon}}_T^{pl} = \dot{\gamma} \, \boldsymbol{\mu}_T$
$\dot{\gamma} = \|\|\boldsymbol{l}\|\|/h \, [\, \nu_N C_N \boldsymbol{N} + \boldsymbol{\nu}_T C_T \boldsymbol{T}] : \dot{\boldsymbol{\varepsilon}}$	$\dot{\gamma} = 1/h \, [\, \nu_N C_N \boldsymbol{N} + \boldsymbol{\nu}_T C_T \boldsymbol{T}] : \dot{\boldsymbol{\varepsilon}}$

each of them is extremely valuable for its own fields of application. While microplane–based continuum models are usually applied to simulate the behavior of larger structures, particle models are believed to provide further inside into complex microstructural phenomena. The comparison presented in this paper was restricted to granular assemblies of equally sized, spherical particles. Moreover, their contacts which are assumed to be distributed uniformly in space. However, this idealization seems to be too restrictive when compared to reality. For more complex studies, a particle model consisting of particles of different size and shape could be applied to determine micromechanical quantities, for example discrete values of a contact distribution function, which could be used as input parameter for a microplane–based finite element simulation. Since the discrete element method itself is usually too expensive to model complex structures, a finite element simulation based on the additional information provided by microstructural analysis can be considered an appropriate alternative.

References

1. P. A. Cundall & O. D. L. Strack, A discrete numerical model for granular assemblies. Géotechnique, **29**, pp. 47–65, 1979
2. R. J. Bathurst & L. Rothenburg, Micromechanical aspects of isotropic granular assemblies with linear contact interactions. J. Appl. Mech., **55**, pp. 17–23, 1988
3. L. Rothenburg & A. P. S. Selvadurai, A micromechanical definition of the Cauchy stress tensor for particulate media. Proceedings of the International Symposium on Mechanical Behavior of Structured Media, ed. Selvadurai, Ottawa, Canada, pp. 469–486, 1981
4. J. Christoffersen, M. M. Mehrabadi, & S. Nemat-Nasser, A micromechanical description of granular material behavior. J. Appl. Mech., **48**, pp. 339–344, 1981
5. N. P. Kruyt & L. Rothenburg, Micromechanical definition of the strain tensor for granular materials. J. Appl. Mech., **118**, pp. 706–711, 1996
6. K. Walton, The effective elastic moduli of a random packing of spheres. J. Mech. Phys. Solids, **35**, pp. 213–226, 1987
7. B. Cambou, P. Dubujet, F. Emeriault, & F. Sidoroff, Homogenization for granular materials. Eur. J. Mech. A / Solids, **14**, pp. 255–276, 1995
8. F. Emeriault & B. Cambou, Micromechanical modelling of anisotropic non–linear elasticity of granular medium. Int. J. Solids & Structures, **33**, pp. 2591–2607, 1996
9. S. C. Chang, Numerical & analytical modelling of granulates. Computer Methods and Advances in Geomechanics, ed. Yuan, Balkema Rotterdam, pp. 105–114, 1997
10. C.-L., Liao, T.-P. Chang, D.-H. Young, & C. S. Chang, Stress–strain relationship for granular materials based on the hypothesis of best fit. Int. J. Solids & Structures, **34**, pp. 4087–4100, 1997
11. A. Drescher & G. de Josselin de Jong, Photoelastic verification of a mechanical model for the flow of a granular material. J. Mech. Phys. Solids, **20**, pp. 337–351, 1972
12. S. C. Chang, Dislocation and plasticity of granular materials with frictional contacts. Powders & Grains 93, ed. Thornton, Balkema Rotterdam, pp. 105–110, 1993
13. O. Mohr, Welche Umstände bedingen die Elastizitätgrenze und den Bruch eines Materials? Zeitschrift des Vereins Deutscher Ingenieure, **46**, pp. 1524–1530, 1572–1577, 1900
14. O. C. Zienkiewicz & G. N. Pande, Time-dependent multilaminate model of rocks. – A numerical study of deformation and failure of rock masses', Int. J. Num. Anal. Meth. Geom., **1**, pp. 219–247, 1977
15. Z. P. Bažant & P. G. Gambarova, Crack shear in concrete: Crack band microplane model. J. Struct. Eng., **110**, pp. 2015–2036, 1984
16. Z. P. Bažant & P. Prat, Microplane model for brittle plastic material: Part I – Theory, Part II – Verification. J. Eng. Mech., **114**, pp. 1672–1702, 1988
17. I. Carol, Z. P. Bažant, & P. Prat, New explicit microplane model for concrete: Theoretical aspects and numerical implementation. Int. J. Solids & Structures, **29**, pp. 1173–1191, 1992
18. E. Kuhl & E. Ramm, On the linearization of the microplane model. Mech. Coh. Fric. Mat., **3**, pp. 343–364, 1998
19. V. A. Lubarda & D. Krajcinovic, Damage tensors and the crack density distribution. Int. J. Solids & Structures, **30**, pp. 2859–2877, 1993
20. K.-I. Kanatani, Distribution of directional data and fabric tensors. Int. J. Eng. Science, **22**, pp. 149–164, 1984
21. S. Luding, M. Lätzel, & H. J. Herrmann, From discrete to continuous granular media. Granular Matter, 2, pp. 123–135, 2000
22. Z. P. Bažant & B. H. Oh, Efficient numerical integration on the surface of a sphere. ZAMM, **66**, pp. 37–49, 1986